JEAS | Journal of Economics and Administrative Sciences
E-ISSN: 2148-1792 P- ISSN: 1302-2024
Volume 5, Supplement Issue 2
www.jeasweb.org

Reduction of Torque Ripple of Flux-Switching Permanent Magnet Machines by Modifying the Structure

Zohreh Bagheri
Master Graduate, Department of Electrical Engineering, Shahed University, Tehran, Iran;

Mohammad Reza Besmi
Associate Professor, Department of Electrical Engineering, Shahed University, Tehran, Iran;

*Pouria Nadri**
Masters Student, Department of Electrical Engineering, Shahed University, Tehran, Iran; (corresponding Author).

ABSTRACT

As one of the electric machines, Flux-Switching Permanent Magnet machines (FSPMs) have been considered by many researchers. Due to the use of low flux densities and low-cost permanent magnets, these machines structurally make it easy to provide power densities similar to conventional high-energy-density PMSMs. Since the structure of flux-switching permanent magnet machines, windings, and permanent magnets are located on the machine stator, it can be considered a combination of the switched reluctance motor (SRM) and induction generators. Research shows that these machines have high power/torque density, better efficiency, and more flux attenuation than PMSM motors. On the other hand, the generated cogging torque is higher than other permanent magnet motors due to the interaction of stator permanent magnets and rotor teeth. This causes vibration, noise, and machine improper performance. The main source of torque ripples in electric machines is cogging torque. Hence, a flux-switching permanent magnet motor is designed with a low torque ripple in the present study. This study aims to reduce cogging torque by different techniques and reduce torque ripple. Necessary simulations were performed with MATLAB software, and the proposed design was optimized using the Taguchi technique. Finally, the 3D finite element method (FEM) was simulated in ANSOFT Maxwell software, and the results were discussed.

Keywords: Torque, Cogging torque reduction, Torque ripple reduction, Permanent magnetic machines, Flux-Switching machines, Optimization, Analytical models.

1. Introduction

Environmental pollution and weather changes are some of the hugest challenges of our generation. Because the role of environmental pollution goes beyond the working range of environmental activists and directly affects people's lives. In order to impose environmental limitations, the use of electric and hybrid vehicles is constantly increasing, and their use has been encouraged by governments [1,2]. The electric machines require the design of structures with features such as high torque at low speed, high power density, high strength, fast torque response, low torque ripple and noise, high reliability, constant power at high speeds, and reasonable cost [3]. On the other hand, magnet-drive brushless machines have been widely developed due to the significant success of permanent magnet materials and power electronic components. Recently, permanent magnet machines with coils and magnets on their stators have been considered by designers due to their unique characteristics such as high strength, high power density, high efficiency, etc. [4]. Flux-Switching Permanent Magnet machines (FSPMs) are a promising option to replace Permanent Magnet Synchronous Machine (PMSM). The advantages of these machines are rotor strength, excellent controllability, smooth torque vibrations, high-density torque production, and higher efficiency. Furthermore, these machines are suitable for applied programs and operation in severe environmental conditions such as wind generators, in which strength is very important [5]. Meanwhile, torque oscillations and torque ripple control for these machines have been one of the main topics in recent research. Because these machines usually have a relatively high torque ripple compared to other conventional brushless permanent magnet machines. In general, three main sources are mentioned in various sources that lead to unwanted torque oscillations, which are: (i) cogging torque due to interactions between the permanent magnet and the gaps of stator and core rotor (ii) harmonics in the waveform of phase back Electro Motive Force (EMF) due to concentrated windings and armature currents attention to the Pulse Width Modulation (PWM), and (iii) variable reluctance torque attention to changes in Dq-axes components in front of the rotor position [6,7]. Meanwhile, cogging torque is the reason for torque ripple, and many scientists have tried to study the relationship between cogging torque and torque ripple with analytical and numerical solving [8]. Flux switching machines and their application in hybrid machines are very clear today. Hence, many articles have studied and designed these machines. The flux switching machine presented in the literature [9] has a structure of 6 stator slots and eight rotor poles (6S-8P). The proposed design for the motor is based on 2D finite element analysis. This study showed that this machine has a better performance and produces more torque and power than a permanent pole synchronous motor. In the literature [10], two different structures of flux switching machines, 12S-10P and 12S-14P in FEFSM type, are studied by applying external drive on the rotor and the characteristics of cogging torque flux distribution, coupling flux, and winding arrangement. The mentioned motor has a more complex structure than the internal drive on the rotor but with fewer losses. In addition, it does not require a permanent pole, which reduces costs. Several articles mention flux-switching permanent magnet machines suffer from relatively high cogging torque due to the prominent pole structure and high air gap flux density, which causes torque ripple, noise, and vibration, especially at high speeds. In order to improve the performance of these machines, several methods have been described in foreign articles. Gathe Dupas et al. proposed a new structure in their paper for hybrid drive in flux-switching machines. The feature of this machine is the components of the drive coil that create a 3D drive flux to control the air gap. In the present paper, a 3D finite element analysis is performed and compared with experimental results. The present model makes it possible to show the active flux route, discover the chargeability of a new structure and determine the effect of material properties [11]. In their paper for DC-drive flux switching machines, Y. Tang et al. proposed a topology to improve the magnetic field weakness in these machines. The machine proposed in the present study maintained the structure of conventional flux switching machines and used DC coils instead of permanent magnets, which improves torque [12]. In other studies, various methods are expressed for reducing cogging torque, such as pole-notching rotor [13], pole flange rotor [14], combined techniques (inner-inner and bridge outer-outer stator lamination) [15]. 12S-7P and 6S-14P models from FSPM with an overlapping winding configuration are also proposed due to having a very high torque density compared to non-overlapping windings in attention to the degree factor correction. Furthermore, the overlapping winding configuration performed in

permanent magnet rotor machines can also minimize the effects of noise and harmonics [16]. Due to the unique structure of flux-switching permanent magnet machines and the interaction of stator permanent magnets and rotor teeth, the cogging torque generated is higher than other permanent magnet motors. This increases torque ripple and leads to vibration, noise, and car poor performance. The main factor in generating cogging torque is the energy change in the motor when the rotor is rotating. Cogging torque is generated even when there is no current in the windings. Proper design of the machine structure reduces vibration and noise of flux-switching permanent magnet machines, improves machine performance, and increases machine strength, power, and efficiency. This study has attempted to provide a design algorithm for flux-switching permanent magnet machines to design a machine sample with a low torque ripple. This paper aims to reduce cogging torque with various techniques to reduce torque ripple. To continue, the designed machine is simulated and validated first in MATLAB software and then through finite element method in ANSOFT Maxwell environment, which is one of the most accurate and reliable methods of analyzing electric machines, and the results are analyzed.

2. Materials and methods

In an analytical method [17], cogging torque is calculated using the following Equation:

Eq. 1.

$$T_{cog}(\alpha)=-\frac{\partial W}{\partial \alpha}=-\frac{\partial}{\partial \alpha}\left(\frac{1}{2\mu_0}\int {F_{pm}}^2(\theta)\,\Lambda^2(\theta,\alpha)\,dV\right)$$

Where, W is the energy stored in the air gap, and α is the angle of the rotor location.

In order to simplify this method, the following items are considered:
i. The iron core permeability is assumed to be infinite.
ii. The permanent magnet leakage flux is ignored.
iii. Magnetic flux changes are considered in the radial direction.

Using Fourier analysis, Eq. 1 is obtained as follows:

Eq. 2.

$${F_{pm}}^2(\theta)=F_{pm0}+\sum_{n=1}^{\infty}F_{pmn}\cos(nN_s\theta)$$

The Fourier series coefficients are as follows:

$$F_{pm0}=\frac{N_s}{\pi}{F_{pm}}^2\theta_{st}$$

Using Fig. 1d, the high air-gap flux density can be represented as Fourier series in Equation 3.

Eq. 3

$$\Lambda^2(\theta,\alpha)=\Lambda_0+\sum_{m=1}^{\infty}\Lambda_m\cos mN_r(\theta+\alpha)$$

To reduce the amount of cogging torque, there are different methods such as rotor tooth-notching, rotor tooth-chamfering, rotor-skewing, etc., which rotor-skewing method is used in this study to reduce cogging torque.
Cogging torque is obtained as follows:

Eq. 4

$$T_{cog}(\alpha)=\sum_{m=1}^{\infty}\{T_{cog}\cos\frac{mN_r(\theta_{st}+\theta_{pm})}{2}\sin(\frac{mN_r\theta_{st}}{2}) \times\sin\frac{mN_r\theta_{rt}}{2}\sin\frac{mN_r\theta_{sk}}{2}\sin\frac{mN_r(\theta_{sk}+2\alpha)}{2}\}$$

Eq. 5

$$T_{cog}=\frac{\pi(R_2^2-R_1^2)}{2\mu_0}\cdot\frac{4F_{pm}^2N_s}{mN_r\pi}\cdot\frac{2\Lambda^2}{m\pi}\cdot\frac{L_a}{\theta_{sk}}$$

According to Equation 4, the effective parameters in calculating cogging torque are θ_{st}, θ_{pm}, θ_{sk}, N_r, and N_S. According to the effective parameters in the cogging torque Equation, the changes related to each parameter are given in MATLAB software in the following. According to Equation 4, different methods for reducing cogging torque are presented in the paper. Next, the simulation and code will be performed in MATLAB, and related graphs will be displayed. In this research, four types of flux-switching permanent magnet motors are used. In all the motors, the number of stator slots was 12, and the number of rotor slots was considered 10, 14, 16, and 20. Although the Least Common Multiple (LCM) values for two machines with the number of rotor slots of 10 and 20 are equal to 60, due to the difference in the Greatest Common Divisor (GCD) values for the number of stator slot and rotor, the cogging torque range in them is different.

Optimal Skewing Factor (θ_{sk}): Values of θ_{sk} which lead to the minimum Equation 4, when $sin\frac{mN_r\,\theta_{sk}}{2}=0$
Rotor Tooth Width (θ_{rt}): Values of θ_{rt} which lead to the minimum cogging torque Equation when we set sine section in the cogging torque Equation (Equation 4) containing θ_{rt} equal to zero.
Stator Tooth Width (θ_{st}): Values of θ_{st} which lead to the minimum cogging torque Equation when we set sine section in the cogging torque Equation (Equation 4) containing θ_{st} equal to zero.
Magnet Thickness: Values of θ_{pm} which lead to the minimum cogging torque Equation when we set sine section in the cogging torque Equation (Equation 4) containing θ_{pm} equal to zero.

Cogging torque reduction based on asymmetric MMF distribution
If the stator teeth are asymmetric, it can be obtained from the following Equation.

Eq. 6

$$F_{pm}{}^2(\theta)=F_{pm0}+\sum_{n_1=1}^{\infty}F_{pmn_1}\cos(\frac{n_1N_s\theta}{2})$$

Where

Eq. 7

$$F_{pm0}=\frac{N_s}{2\pi}(F_{pm1}{}^2\theta_{st1}+F_{pm2}{}^2\theta_{st2}) \quad , \quad F_{pmn_1}=\frac{2}{n_1\pi}$$
$$\{F_{pm1}{}^2[\sin\left(\frac{n_1N_s\theta_{pm}}{4}+\frac{n_1N_s\theta_{st1}}{2}\right)-\sin\left(\frac{n_1N_s\theta_{pm}}{4}\right)]+$$
$$F_{pm2}{}^2[\sin\left(n_1\pi-\frac{n_1N_s\theta_{pm}}{4}\right)-\sin\left(n_1\pi-\frac{n_1N_s\theta_{pm}}{4}-\frac{n_1N_s\theta_{st2}}{2}\right)]\}.$$

Asymmetric Stator Slot (ASS)
In this method, cogging torque reduction is converted to the following Equation.

Eq. 8

$$F_{pm}{}^{2}(\theta)=F_{pm0}+\sum_{n_2=1}^{\infty} F_{pmn_2}\cos(\frac{n_2N_s\theta}{2})$$

Where

Eq. 9

$$F_{pmn_2}=\frac{4}{n_2\pi}\sin\left(\frac{n_2N_s\theta_{st}}{4}\right)[F_{pm1}{}^{2}\cos\left(\frac{n_2N_s\theta_{s1}}{4}+\frac{n_2N_s\theta_{st}}{4}\right)+ F_{pm2}{}^{2}\cos\left(n_2\pi-\frac{n_2N_s\theta_{s2}}{4}-\frac{n_2N_s\theta_{st}}{4}\right)],\ F_{pm0}=\frac{N_s\theta_{st}}{\pi}\left(F_{pm1}{}^{2}+F_{pm2}{}^{2}\right).$$

Cogging torque reduction based on asymmetric magnetic permeance distribution

Rotor with asymmetric slot

The magnetic permeability graph of the rotor relative to the location of the Fourier series rotor. The magnetic permeability is obtained from Equation 9.

Eq. 10

$$\Lambda^{2}(\theta,\alpha)=\Lambda_{01}+\sum_{m_1=1}^{\infty}\Lambda_{m_1}\cos\frac{m_1N_r}{2}(\theta+\alpha)$$

$$\Lambda_{m_1}=\begin{cases}\frac{2\Lambda^{2}}{m_1\pi}[\sin\frac{m_1N_r}{2}(\frac{\theta_{r1}}{2}+\theta_{rt})-\sin\frac{m_1N_r\theta_{r1}}{4}+ \sin(\frac{m_1N_r\theta_{r2}}{4})-\sin\frac{m_1N_r}{2}(\frac{\theta_{r2}}{2}+\theta_{rt})], & m_1 \text{ is odd}\\ \frac{2\Lambda^{2}}{m_1\pi}[\sin\frac{m_1N_r}{2}\left(\frac{\theta_{r1}}{2}+\theta_{rt}\right)-\sin\frac{m_1N_r\theta_{r1}}{4}- \sin(\frac{m_1N_r\theta_{r2}}{4})+\sin\frac{m_1N_r}{2}(\frac{\theta_{r2}}{2}+\theta_{rt})], & m_1 \text{ is even}\end{cases}$$

Using Equation 10 and placing it in Equation 4, the magnetic torque Equation based on the rotor asymmetric slot model will be obtained.

Meshing*:* After drawing the motor geometry, its various components will mesh. In order to mesh the motor structure, each of its components is separately selected. Then, the appropriate mesh for it will be defined according to the available tools in the software. The desired motor mesh is shown in Fig.1.

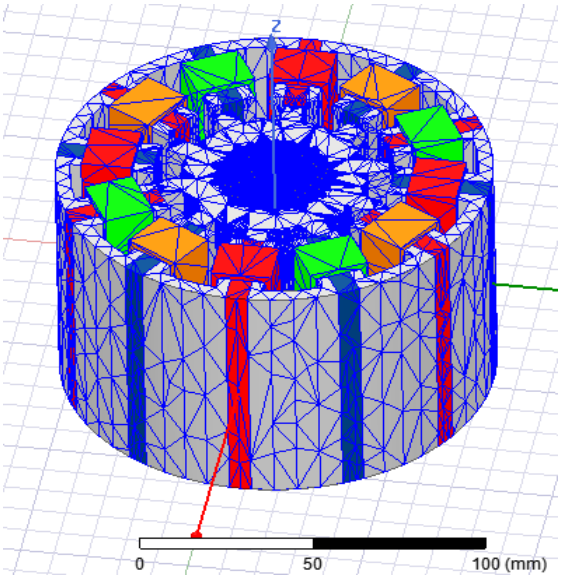

Fig.1. Meshing of flux-switching motor

The available tool in MAXWELL was used to draw the desired motors in the software. The drawing is automatically done in this tool by selecting the appropriate model and entering the motor information**.** The magnet used in the motors is made of Neodymium 35. The driving of the flux-switching motor is defined as three balanced sine sources with a phase difference of 120°. To calculate motor torque in the present investigation, motor windings are driven by a current rating or a voltage rating, and the speed rating of the rotor is defined. The torque that is read in the output in this state is called torque rating. In order to optimize, first, the dimension of the motor structure is selected as a parameter, and the best state is determined by changing this parameter and studying the motor behavior in terms of selected parameter changes. The selected optimization algorithm is Taguchi.

Determining of optimization variables and constraints

The optimization variables are first determined before optimizing the motor. These parameters for the motor include rotor skewing factor (θ_{sk}), rotor tooth width (θ_{rt}), stator tooth width (θ_{st}), and magnet thickness (θ_{pm}). In the next step, each of the mentioned parameters will change in levels, and the motor behavior will be studied in terms of these changes. The levels considered for the desired parameters are listed in Table 1.

Table 1. Changes levels for motor parameters

12/10	***Level 1***	***Level 2***	***Level 3***	***Level 4***
θ_{sk}	6.3	12.3	18	19
θ_{rt}	1.7	4.7	6.8	7
θ_{st}	0.23	1.7	8	9
θ_{pm}	0.87	1.1	9.7	10.27
12/14	***Level 1***	***Level 2***	***Level 3***	***Level 4***
θ_{sk}	4	6	8	13
θ_{rt}	1.8	4	6.14	6.7
θ_{st}	3.4	4	7.3	8
θ_{pm}	1.26	3.4	9.8	10

Steps of Taguchi technique

Taguchi technique corresponding to parameters and levels are shown in Table 2. 16 experiments have been proposed in the Taguchi technique according to the number of levels and parameters. In total, 44 different experiments are possible, reduced to 16 experiments using the Taguchi technique. The numbers shown in Table 2 indicate the desired parameter level. For example, the first line represents $A_1B_1C_1D_1$,

which indicates that the first level values are selected for the parameters in the first experiment, and the motor outputs are calculated.

Table 2. Taguchi experiments combination

Parameter / Examination	θ_{sk}	θ_{rt}	θ_{st}	θ_{pm}
1	1	1	1	1
2	1	2	2	2
3	1	3	3	3
4	1	4	4	4
5	2	1	2	3
6	2	2	1	4
7	2	3	4	1
8	2	4	3	2
9	3	1	3	4
10	3	2	4	3
11	3	3	1	2
12	3	4	2	1
13	4	1	4	2
14	4	2	3	1
15	4	3	2	4
16	4	4	1	3

3. Results

The flux density of the motor structure

The flux density distribution and the motor flux path with a structure of 12/10 are shown in Fig. 2. It can be observed that the flux density for the stator hot spot is about 3.145 T, which corresponds to the sharp points. Furthermore, it is observed that the core flux density is about 1.6 T, which is less than the core saturation value. According to Fig. 2b, it can be observed that the flux density for the stator hot spot is about 3.284 T, which corresponds to the sharp points. Furthermore, it is observed that the core flux density is about 1.6 T, which is less than the core saturation value.

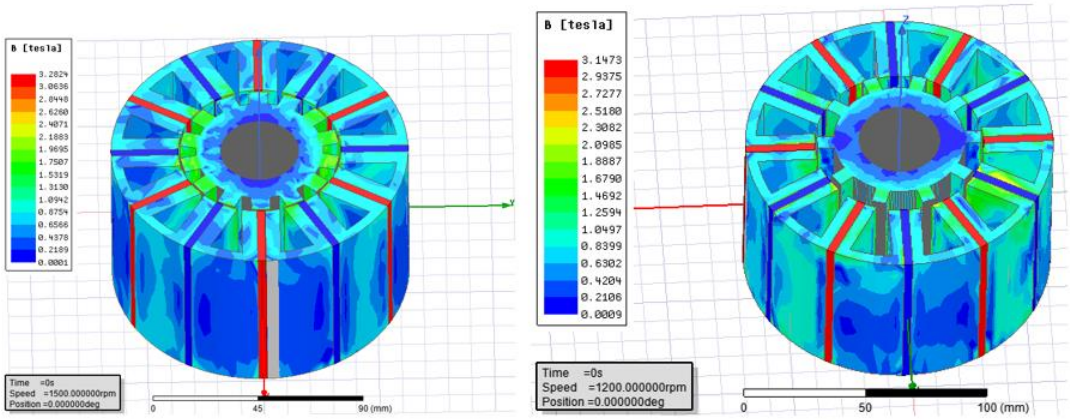

Fig. 2. Flux density of motor with a structure of (a) 12/10 and (b) 12/14

Investigation of the simulation results

Test results for the flux-switching motor with a structure of 12/10

Using the results of experiments designed by the Taguchi technique and after analyzing the experiment results, the optimal combination of factors levels and torque values at the optimal point is calculated. According to the obtained optimal point, the required corrections to reach the optimal point are made, and the simulation results are compared with the results obtained by the Taguchi technique. The results of different experiments are given in Table 3. In the next step, each level effect must be separately calculated. For example, to calculate the effect of the first level of the parameter of θ_{sk} (θ_{sk1}), the average of experiments of 1, 2, 3, and 4 must be calculated. By drawing the output graph for different levels of each parameter, Fig. 3a is obtained. According to Fig. 3, the best combination for the optimal air gap flux density mode is (θ_{pm3}, θ_{st3}, θ_{rt4}, θ_{sk2}). In addition, according to Table 3, the best combination for the optimal cogging torque state is the state (θ_{pm1}, θ_{st1}, θ_{rt1}, θ_{sk3}). Thus, the final levels will be (θ_{pm3}, θ_{st4}, θ_{rt4}, θ_{sk4}).

Table 3. Results of Taguchi different experiments

Experiment	Air gap flux density (T)	Cogging torque (N.m)
1	0.029	50
2	0.736	1.596
3	1.084	1.338645
4	1.367	1.3965
5	1.515	0.464835
6	1	0.835905
7	0.074	0.13965
8	1.453	1.198995
9	0.93	0.00001995
10	0.987	1.995
11	0.27	0.00000000049875
12	0.062	0.02394
13	0.17	0.0596505
14	0.91	0.01995
15	0.4	1.50024
16	0.774	0.560595
Average	0.735063	0.696243778

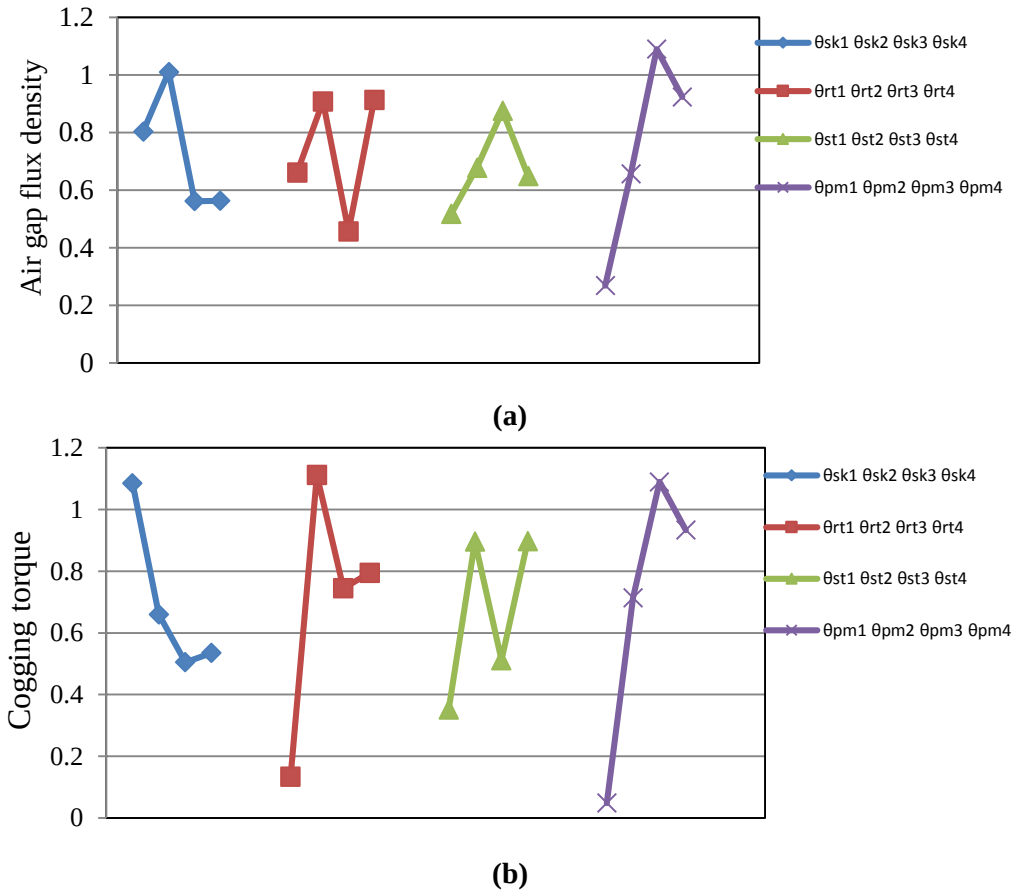

Fig. 3. (a) The effect of factor levels on the air gap flux density (b) the effect of factor levels on cogging torque

Test results for the flux-switching motor with a structure of 12/14

Following a similar pattern as before, the simulation results of different experiments are listed in Table 4. By drawing the output graph for different levels of each parameter, we reach Fig. 4. According to Fig. 4a, the best combination for the optimal state of air gap flux density is (θ_{pm3}, θ_{st3}, θ_{rt2}, θ_{sk2}). In addition, according to Fig. 4b, the best combination for the optimal cogging torque state is (θ_{pm1}, θ_{st4}, θ_{rt3}, θ_{sk4}). According to these two optimal states, it is observed that there is no common state, so in this state, the effect of each parameter on the cogging torque and air gap flux density must be calculated. Similar to the previous state, we consider the fourth level for the curvature angle of the rotor (θ_{sk4}). As air gap flux density decreases, we will compensate for this decline by selecting the appropriate levels for the other parameters. Thus, the final levels will be (θ_{pm3}, θ_{st3}, θ_{rt2}, θs_{k4}).

Table 4. Results of different experiments

Experiment	Air gap flux density (T)	Cogging torque (N.m)
1	0.029	0.04268544
2	0.736	0.5
3	1.084	0.6
4	1.367	0.37632
5	1.515	0.849408
6	1	0.999936
7	0.074	0.056448
8	1.1	0.6461952
9	0.93	0.193536
10	0.987	0.2591232
11	0.27	0.2053632
12	0.062	0.04053504
13	0.17	0.04655616
14	0.91	0.008580096
15	0.4	0.03462144
16	0.774	0.09010176
Average	0.713	0/309338096

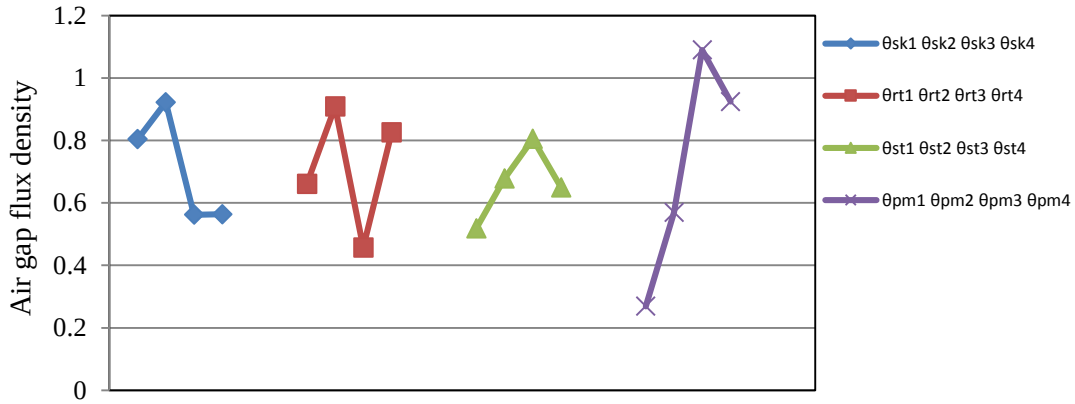

(a)

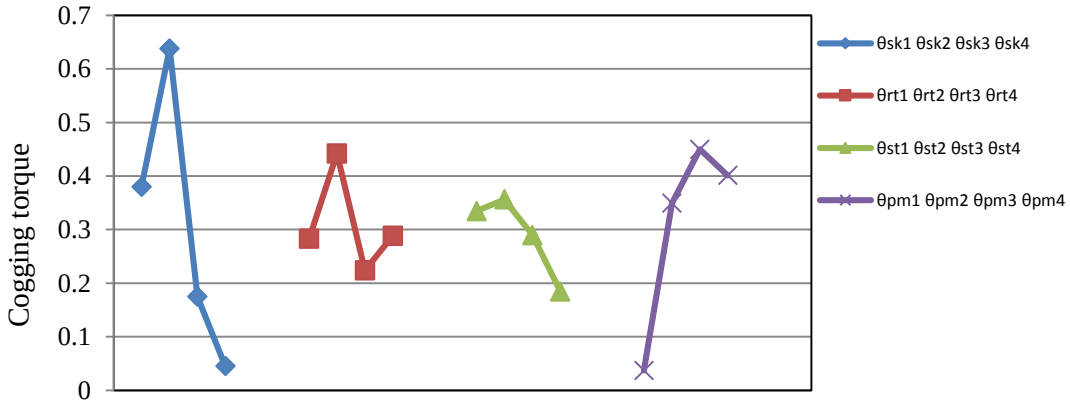

(b)

Fig. 4. (a) The effect of factor levels on the air gap flux density (b) The effect of factor levels on cogging torque

Optimization results

Cogging torque graph, torque, and air gap flux density in two different states for 12/10 motor

The motor cogging torque in the initial and optimized state is shown in Fig. 5a. The cogging torque in the optimal state is about 1.4 N.m less than the initial state. It means that the cogging torque is reduced by about 51%. On the other hand, we know that the skewing of the rotor reduces the motor performance. Hence, in addition to the cogging torque, the motor air gap flux density is compared in two states, as shown in Fig. 5b. It is observed in this figure that despite the changes in the motor structure, the motor air gap flux density has been almost unchanged.

Furthermore, the B-EMF of the motor in this state is as shown in Fig. 5c. In this state, the maximum voltage is about 10 V lower than the previous state, whereas the harmonics have decreased. Finally, the torque curve of the optimized motor by the main motor is shown in Fig. 5d. By comparing these two figures, it can be seen that the torque ripple has improved.

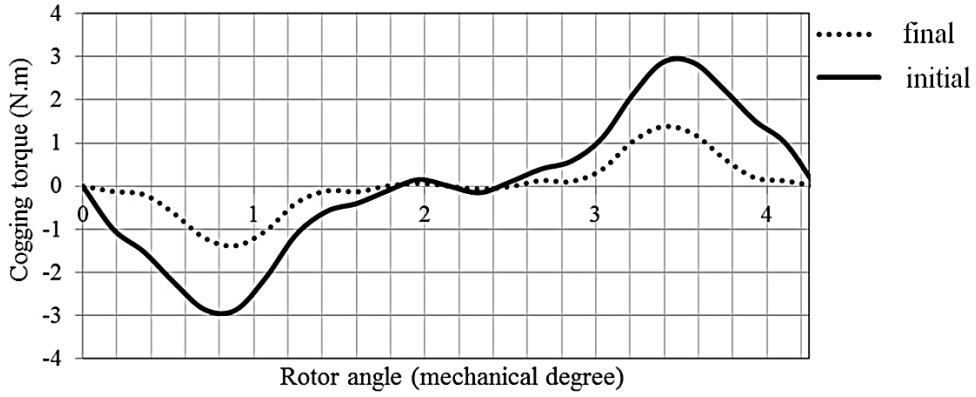

(a)

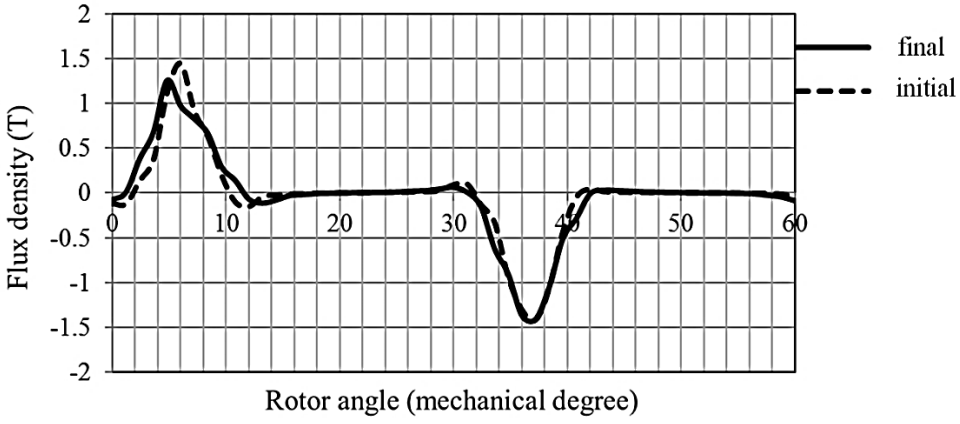

(b)

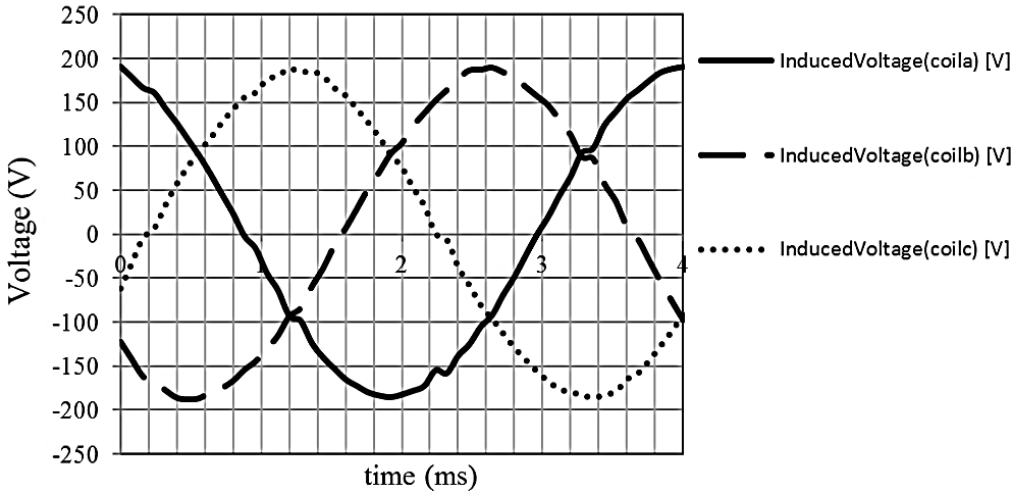

(c)

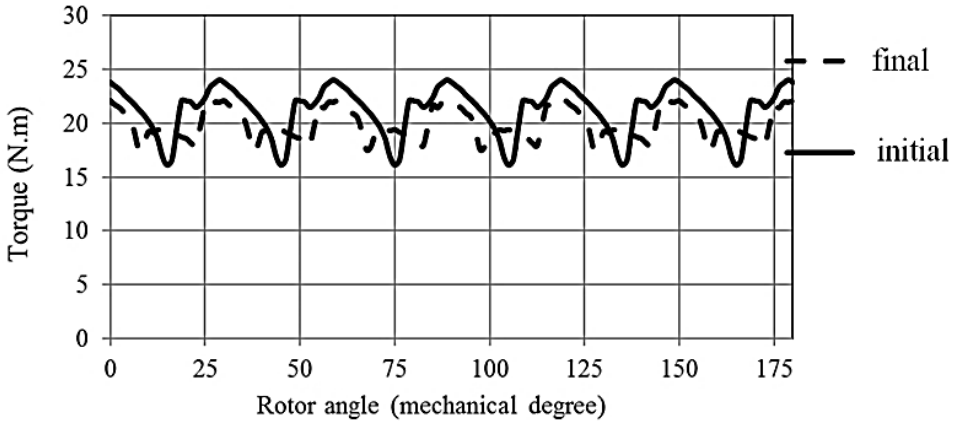

(d)

Fig. 5. (a) Cogging torque graph in the two initial and final states for a structure of 12.10 (b) Air gap flux density in the two states (c) B-EMF in the optimal state, and (d) Comparison of the optimal motor torque with the main motor torque

Cogging torque graph, torque, and air gap flux density in two different states for 12/14 motor

The motor cogging torque in the initial and optimized state is shown in Fig. 6a. As shown, the cogging torque in the optimal state is about 0.4 N.m less than the initial state. It means that the cogging torque is reduced by about 55%. The motor air gap flux density in this structure is similar to the previous structure, shown in Fig. 6b. Furthermore, the B-EMF of the motor in this state is shown in Fig. 6c. It can be observed that harmonics are decreased in this state. Finally, the optimized motor torque curve by the main motor is shown in Fig. 6d. By comparing these two figures, it can be found that the torque ripple has improved.

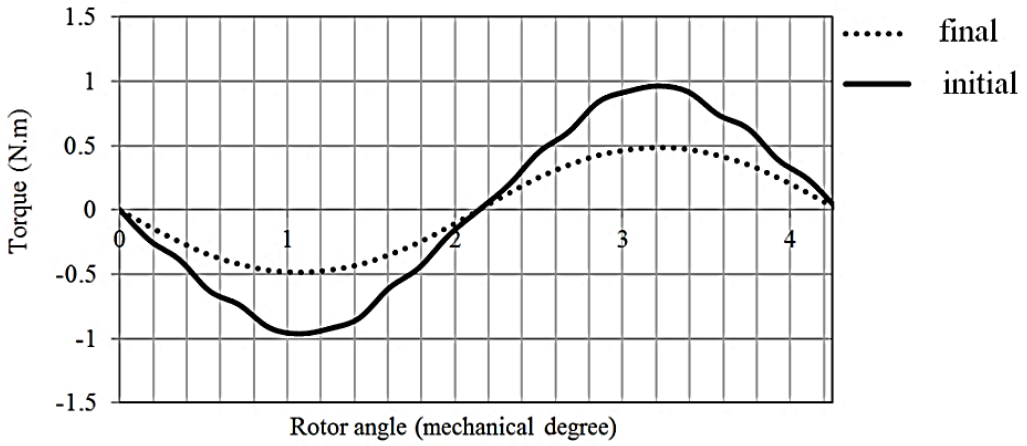
Torque (N.m)
Rotor angle (mechanical degree)
final
initial

(a)

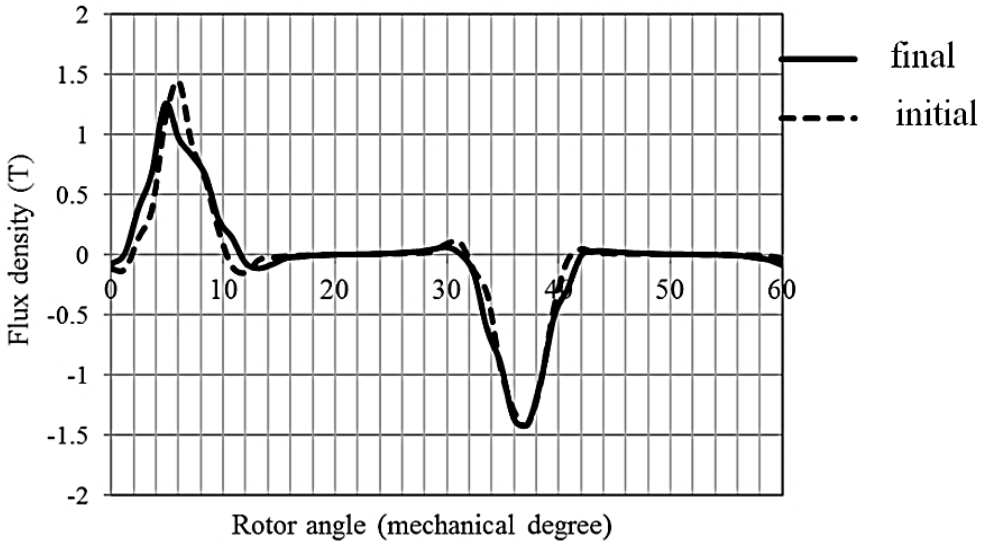
Flux density (T)
Rotor angle (mechanical degree)
final
initial

(b)

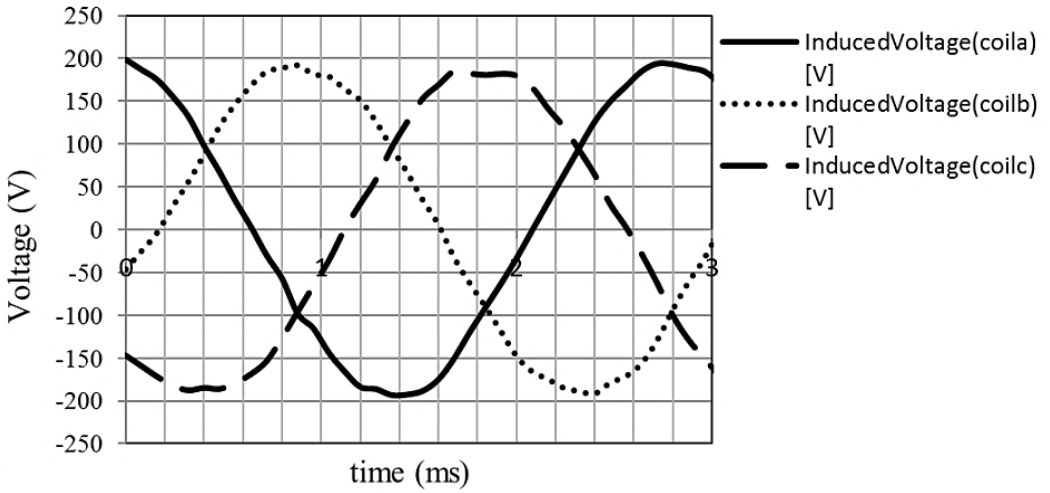
Voltage (V)
time (ms)
InducedVoltage(coila) [V]
InducedVoltage(coilb) [V]
InducedVoltage(coilc) [V]

(c)

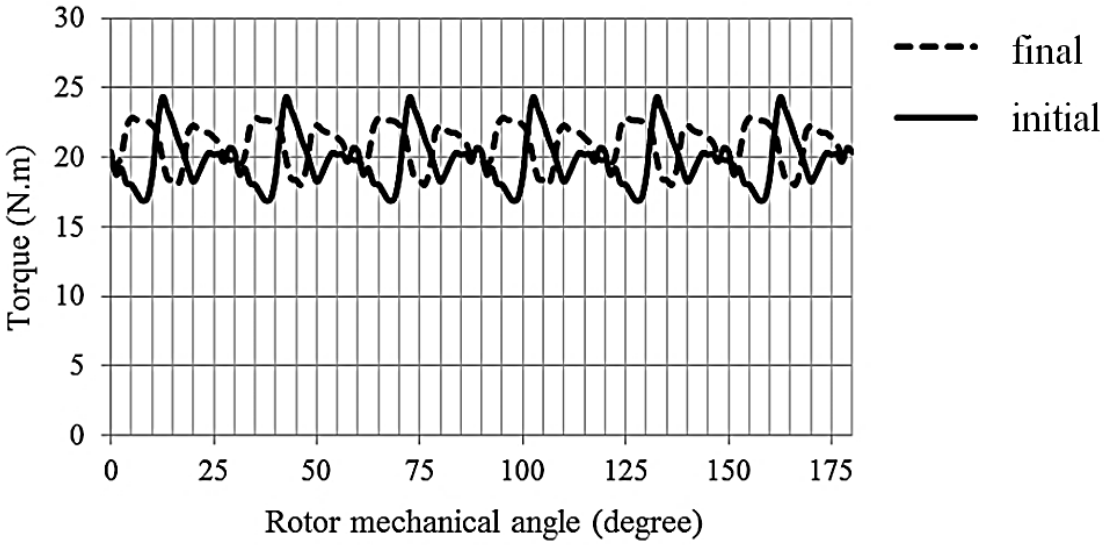

(d)

Fig. 6. (a) Cogging torque graph in the two initial and final states for a structure of 12.14 (b) Air gap flux density in the two states (c) B-EMF in the optimal state, and (d) Comparison of the optimal motor torque with the main motor torque

4. Conclusions

One of the methods for reducing cogging torque and torque ripple is rotor skewing. Simulation using the 3D finite element method is more accurate but slower than 2D. Hence, the 2D or 3D finite element method can be chosen depending on the importance of simulation accuracy and speed. In the present investigation, we preferred accuracy to speed and used the 3D finite element method to simulate the optimal motor. The Taguchi technique is one of the best techniques to get an optimal compound for a motor and reach the optimal point. According to the studies and compare the test results on the cogging torque of the motor in the initial and optimal state, the cogging torque in the optimal state for the motor with a structure of 12/10 was about 1.4 N.m and for the motor with a structure of 12/14 was about 0.4 N.m less than the initial state. It means that the cogging torque is reduced by about 51% for a structure of 12/10 and by about 55% for 12/14. Skewing the rotor reduces the motor performance. Hence, in addition to the cogging torque, the motor air gap flux density was calculated in both initial and optimal states, and it was observed that despite the changes in the motor structure, the motor air gap flux density for both structures of 12/10 and 12/14 was unchanged. Furthermore, the B-EMF of the motor was calculated in both initial and optimal states in which the maximum voltage for both motor structures of 12/10 and 12/14 was about 10 V lower than the initial state, whereas the harmonics were decreased. Finally, the torque curve of the optimized motor is calculated by the initial motor, and it was observed that the torque ripple has improved .

References

Kuri, B., Li, F. Allocation of Emission Allowances to Effectively Reduce Emissions in Electricity Generation. IEEE Power & Energy Society General Meeting. PP: 1-8, 2009.

Xu Ran Li and et al. A multimarket decision-making framework for GENCO considering emission trading scheme. IEEE Transactions on Power Systems. Vol. 28, No. 4, PP: 4099 – 4108, 2013.

Z. Q. Zhu and D. Howe, "Electrical machines and drives for electric, hybrid, and fuel cell vehicles," Proceedings of the IEEE, vol.95, pp.746-765, 2007.

S. E. Rauch and L. J. Johnson, "Design principles of flux-switching alternators," AIEE Trans., vol. 74III, pp. 1261–1268, 1955.

A.Kumar, A.Srivastava, "Performance Investigation of Various Flux-Switching Machines for Hybrid Electric Vehicles: A Review"; International Journal of Advanced Research in Electrical, Electronics and Instrumentation Engineering, Vol. 5, Issue 12, 2016.

T. M. Jahns and W. L. Soong, "Pulsating torque minimization techniques for permanent magnet AC motor drives-a review," IEEE Trans. Ind. Electron., vol. 43, no. 2, pp.321-330, Apr. 1996.

J. X. Shen and W. Z. Fei, "Permanent magnet flux switching machines- topologies, analysis and optimization," in Proc. of 4th Int. Conf. Power Eng., Energy and Elect. Drives, Istanbul, Turkey, May, 2013, pp. 352-366.

Xiaofeng Zhu and et al, "Analytical Approach for Cogging Torque Reduction in Flux-Switching Permanent Magnet Machines Based on Magneto Motive Force-Permeance Model", IEEE Transactions on Industrial Electronics, 2018.

Shahabuddin Afrasiabi, Davood Keshavarzpour, Mohsen Norouzi, Pedram Ghaleh Bani, Design of flux switching motor with hybrid excitation using 2D finite element analysis, The Second National Conference on Applied Research in Electrical Engineering, Mechanics and Mechatronics.

Shahabuddin Afrasiabi, Hossein Keshtkar, Pedram Ghalebani, Design of flux switching engine with different structure for use in hybrid cars using two-dimensional finite element analysis, Second National Conference on Applied Research in Electrical Engineering, Mechanics and Mechatronics.

Agathe Dupas, Sami Hlioui, Emmanuel Hoang, Mohamed Gabsi, and Michel Lecrivain, "Investigation of a New Topology of Hybrid-Excited Flux-Switching Machine with Static Global Winding: Experiments and Modeling," IEEE Transactions on Industry Applications, Vol. 52, No. 2, March/April, 2016.

Y. Tang, J. J. H. Paulides, T. E. Motoasca, and E. A. Lomonova, "Flux-Switching Machine with DC Excitation", IEEE Transactions on Magnetics, V. 48, N. 11, November 2012.

Z.Q. Zhu and J. Chen, "Advanced flux-switching permanent magnet brushless machines," IEEE Transactions on Magnetics, vol. 46, pp. 1447-1453, 2010.

C. Sikder, I. Husain, and W. Ouyang, "Cogging torque reduction in flux-switching permanent-magnet machines by rotor pole shaping," IEEE Transactions on Industry Applications, vol. 51, pp. 3609-3619, 2015.

M. Shen, J. Wu, C. Gan, Y. Hu, and W. Cao, "Cogging torque reduction in FSPM machines with short magnets and stator lamination bridge structure," in Industrial Electronics Society, IECON 2016-42nd Annual Conference of the IEEE, 2016, pp. 4307-4312.

L. Shao, W. Hua, Z.Q. Zhu, X. Zhu, M. Cheng, and Z. Wu, "A Novel Flux-Switching Permanent Magnet Machine with Overlapping Windings," IEEE Transactions on Energy Conversion, vol. 32, 2017, pp. 172-183.

X. Zhu, W. Hua, Z. Wu, W. Huang, H. Zhang, and M. Cheng, "Analytical approach for cogging torque reduction in flux-switching permanent magnet machines based on magnetomotive force-permeance model," IEEE Trans. Ind. Electron., vol. 65, no. 3, pp. 1965–1979, 2017.